[redacted]
12/10/97

LOG
12/10/97

Closed-loop Control of Functional Neuromuscular Stimulation

NIH Neuroprosthesis Program Contract Number N01-NS-6-2338
Quarterly Progress Report #6
July 1, 1997 to Sept. 30, 1997

Investigators:
Patrick E. Crago, Ph.D.
Clayton L. Van Doren, Ph.D.
Warren M. Grill, Ph.D.
Michael W. Keith, M.D.
Kevin L. Kilgore, Ph.D.
Joseph M. Mansour, Ph.D.
P. Hunter Peckham, Ph.D.
David L. Wilson, Ph.D.

Departments of
Biomedical Engineering,
Mechanical and Aerospace Engineering,
and Orthopaedics
Case Western Reserve University
and MetroHealth Medical Center

THIS QPR IS BEING SENT TO YOU BEFORE IT HAS BEEN REVIEWED BY THE STAFF OF THE NEURAL PROSTHESIS PROGRAM.

Table of Contents

1. SYNTHESIS OF UPPER EXTREMITY FUNCTION 3

1. a. BIOMECHANICAL MODELING: PARAMETERIZATION AND VALIDATION 3
Purpose 3
Report of progress 3
1. a. i. MOMENT ARMS VIA MAGNETIC RESONANCE IMAGING 3
Abstract 3
Report of Progress 3
Plans for next quarter 7
1.a.ii. PASSIVE AND ACTIVE MOMENTS 7
Abstract 7
Purpose 8
Report of Progress 8
Plans for Next Quarter 14

1. b. BIOMECHANICAL MODELING: ANALYSIS AND IMPROVEMENT OF GRASP OUTPUT 14
Abstract 14
Objective 14
Report of Progress 14
Plans for Next Quarter 19
References 19

2. CONTROL OF UPPER EXTREMITY FUNCTION 20

2. a. HOME EVALUATION OF CLOSED-LOOP CONTROL AND SENSORY FEEDBACK 20
Abstract 20
Purpose 20
Report of Progress 20
Plans for Next Quarter 20

2. b. INNOVATIVE METHODS OF CONTROL AND SENSORY FEEDBACK 20
2. b. i. ASSESSMENT OF SENSORY FEEDBACK IN THE PRESENCE OF VISION 20
Abstract 20
Purpose 21
Report of Progress 21
Plans for Next Quarter 21
2. b. ii. INNOVATIVE METHODS OF COMMAND CONTROL 21
Abstract 24
Purpose 24
Report of Progress 24
Plans for Next Quarter 26
2. b. iii . INCREASING WORKSPACE AND REPERTOIRE WITH BIMANUAL HAND GRASP 26
Abstract 26
Plans for Next Quarter
2. b. iv CONTROL OF HAND AND WRIST 27
Abstract 27
Purpose 27
Report of progress 27
Plans for next quarter 33

1. SYNTHESIS OF UPPER EXTREMITY FUNCTION

The overall goals of this project are (1) to measure the biomechanical properties of the neuroprosthesis user's upper extremity and incorporate those measurements into a complete model with robust predictive capability, and (2) to use the predictions of the model to improve the grasp output of the hand neuroprosthesis for individual users.

1. a. BIOMECHANICAL MODELING: PARAMETERIZATION AND VALIDATION

Purpose

In this section of the contract, we will develop methods for obtaining biomechanical data from individual persons. Individualized data will form the basis for model-assisted implementation of upper extremity FNS. Using individualized biomechanical models, specific treatment procedures will be evaluated for individuals The person-specific parameters of interest are tendon moment arms and lines of action, passive moments, and maximum active joint moments. Passive moments will be decomposed into components arising from stiffness inherent to a joint and from passive stretching of muscle-tendon units that cross one or more joints.

Report of progress

1. a. i. MOMENT ARMS VIA MAGNETIC RESONANCE IMAGING

Abstract

In this quarter, the 3 methods for evaluating tendon moment arm were compared on 4 subjects, each measured 2 times. The three methods were: (1) a 3D tendon excursion method that extended the method of Landsmeer, (2) a 3D geometric method whereby the moment arm was the shortest distance between the joint axis of rotation and the tendon path, and (3) a 2D geometric method whereby single image slices were analyzed. The moment arm of the flexor digitorum profundus at the third metacarpophalageal (MCP) joint was measured. Repeating the imaging and measurement process, the 3D tendon excursion method was more reproducible than the 3D geometric method, and both were much more reproducible than the 2D geometric method. The average percent difference of the 3D tendon excursion data was 10%. Data from the 3D geometric and the 3D tendon excursion methods were reasonably similar despite the fact that the analysis was much different. This enhances our confidence in the measurements. There is a tendency for moment arm to increase with flexion.

Report of Progress

As described previously, we are testing methods for measuring tendon moment arm in the MCP joints of the fingers. We consider this joint to be simpler than the wrist; hence, we elect to study it first. We use high-resolution, 3D MRI to measure tendon moment arm, and our initial goal is to determine an accurate, practical method. As described in the proposal, we are examining 3 methods for analyzing tendon moment arm. They are: tendon excursion, 3D geometric, and 2D geometric.

We now have a total of 4 subjects, each measured on two days. The following is an analysis of these data.

Moment arms obtained from the 3D tendon excursion method are very repeatable with an average percent difference of 10% (Figure 1.a.i.1). In all but one case (AZ at 25 deg), there is less that a 15% difference between the two measurements. In all 8 experiments, the moment arm tends to increase with increasing joint angle, and this increase is greater than the difference between one imaging session and another. The largest moment arm is 19 mm and the smallest is 8.5 mm. Hence, the difference from one subject to another is also much greater than the variability in the measurement.

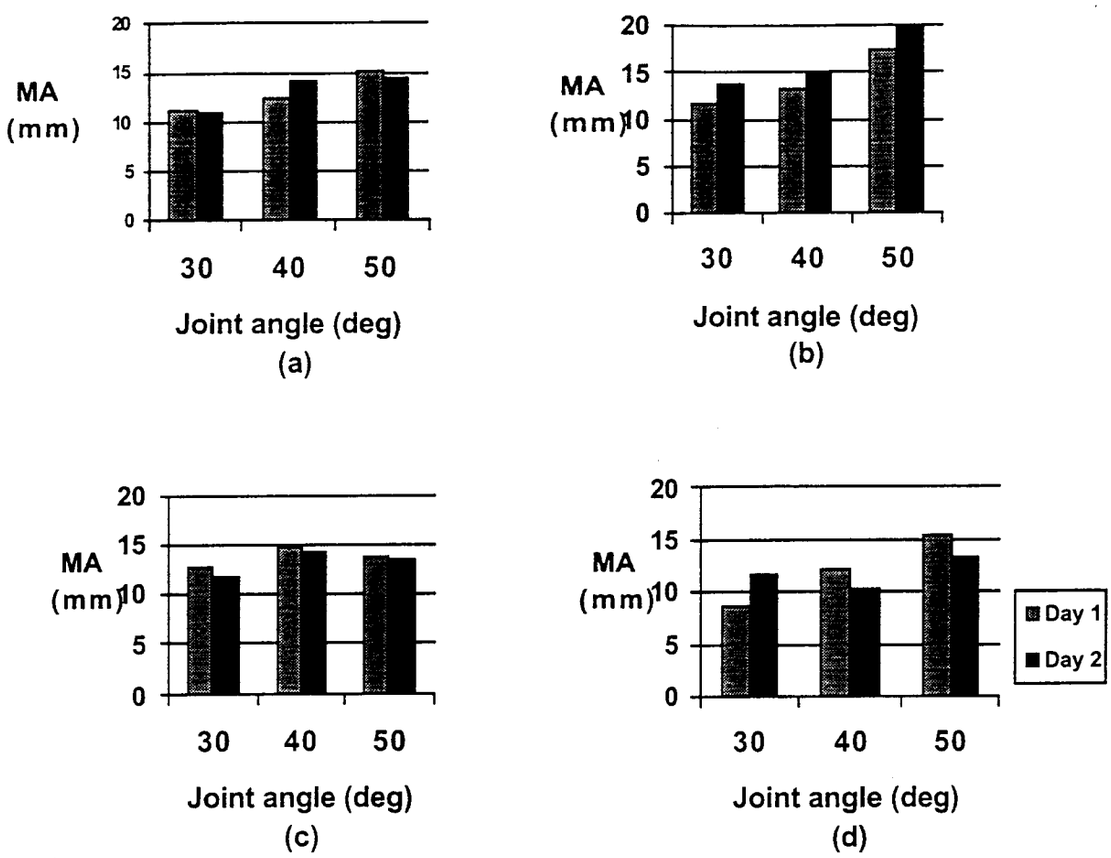

Figure 1.a.i.1. Moment arms (MA) are measured as a function of joint angle using the 3D tendon excursion method. To examine measurement repeatability, complete sets of MR images are obtained on two different days. Image data are analyzed by a single operator. Panels (a), (b), (c), and (d) are results from four different subjects (JK, QZ, RM, and AZ, respectively). Moment arms are very repeatable with the largest and average differences of 25% and 10%, respectively. Each moment arm calculation required measurements from image data sets at two joint angles. For example, we obtained image data nominally at 25 and 35 deg and plotted this value at 30 deg.

The 3D geometric method is less repeatable than the 3D tendon excursion, although most differences are less than 25% with this method (Figure 1.a.i.2). Once again, with the exception of panel (d) day 1, there is a trend toward increasing moment arm as angle increases. Examination of raw image data showed that the quality of images from this particular data set are inferior probably due to an increased distance to the imaging coil center, and we speculate that segmentation error may explain this inconsistent result.

The 3D geometric measurements are consistent with expectations. In almost all cases, the joint axis of rotation lay in the distal head of the metacarpal bone. Most of the axes of rotation are well within 20 degrees of a vector normal to what we consider the plane of motion. Typically, translation in the helical axis analysis is less than 1 voxel.

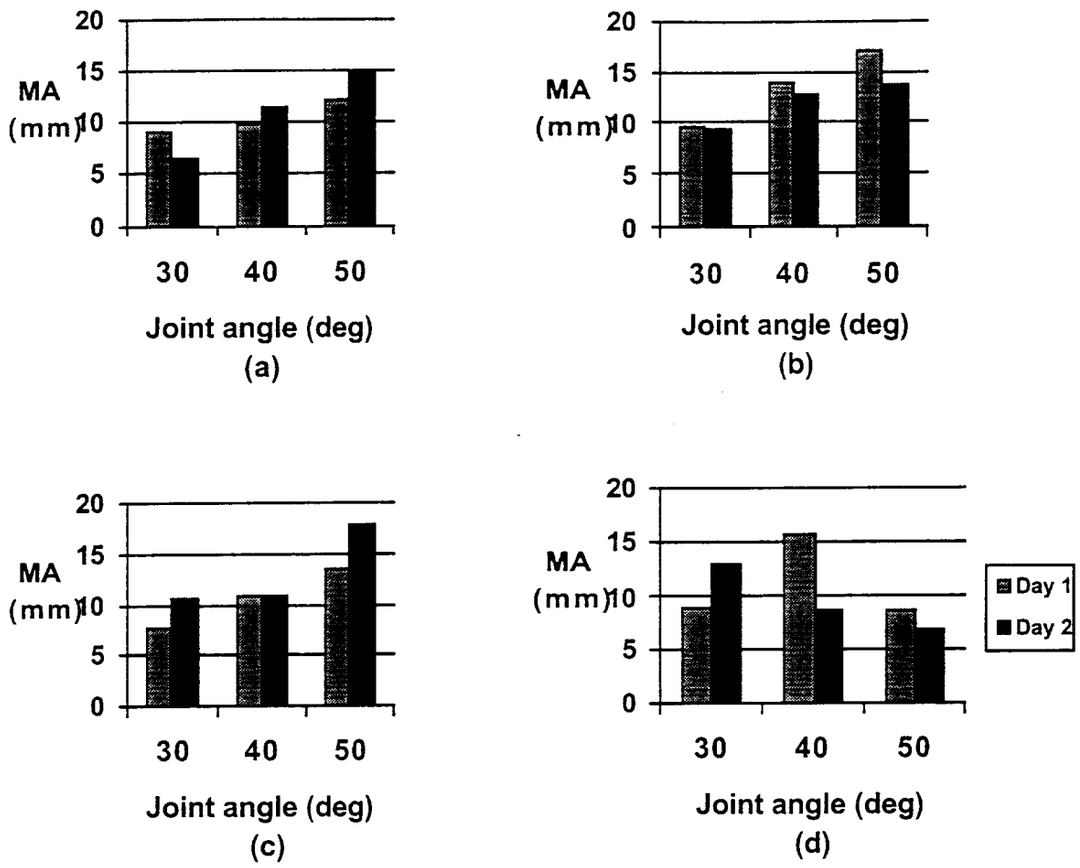

Figure 1.a.i.2. The 3D geometric method is applied to the same image data sets used in Figure 1.a.i.1. As compared to the 3D tendon excursion method, measurements are less repeatable with an average percent difference of 20%. See Figure 1.a.i.1 for other details.

The 2D geometric method is considerably less repeatable than the other methods (Figure 1.a.i.3). From day 1 to day 2, we find variation as much as 75%. We find that the position of the center of rotation changes dramatically as one chooses different anatomical markers. Considering the 3D geometric method to give the true centers of rotation, most of the variability of the 2D method arises from errors in determining the center of rotation.

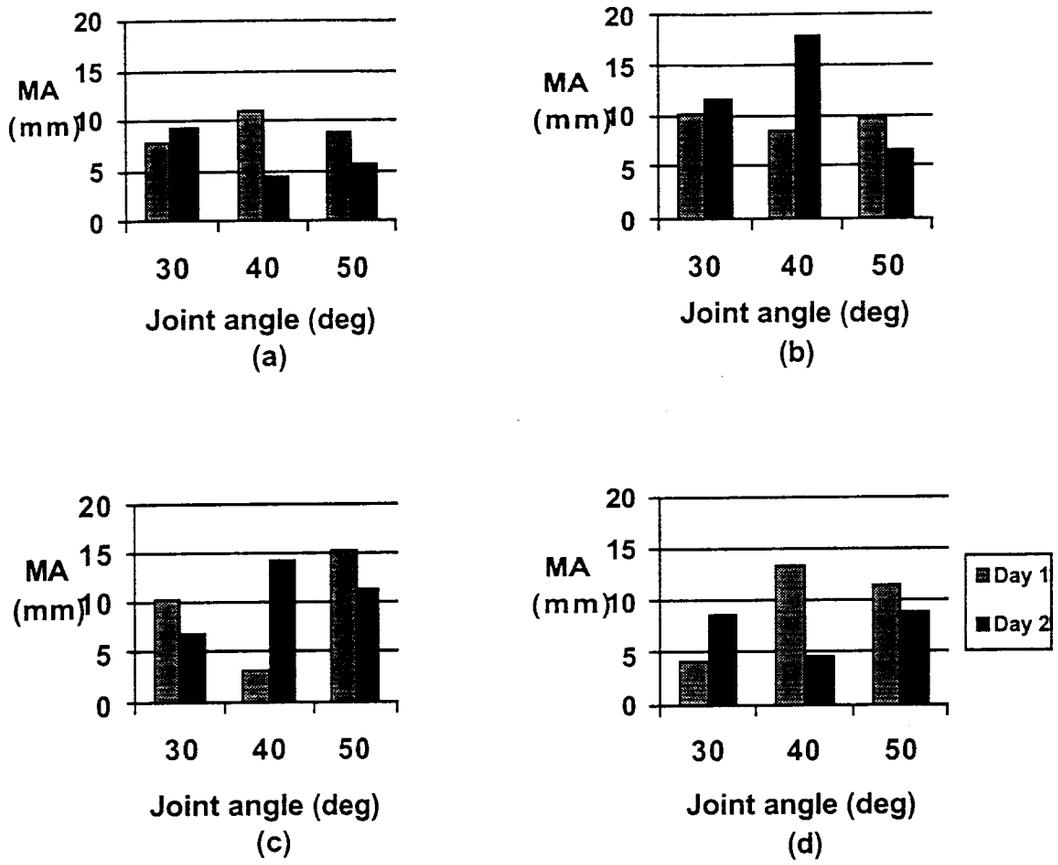

Figure 1.a.i.3. The 2D geometric method is applied to the same image data sets used in Figure 1.a.i.1. The 2D geometric method is not very repeatable with the largest error around 76% and an average difference of 40%. See Figure 1.a.i.1 for other details.

In Figure 1.a.i.4, we compare the 3 methods by plotting data averaged over the two measurements. For the 3D tendon excursion and 3D geometric methods, moment arms tend to increase with joint flexion. With the exception of two cases in panel (d), the 3D tendon excursion method gives moment arm values which exceed those of the 3D geometric method. This is probably due to the angle averaging effect of the tendon excursion method. Values from a 2D evaluation vary considerably and are not comparable to the other two methods.

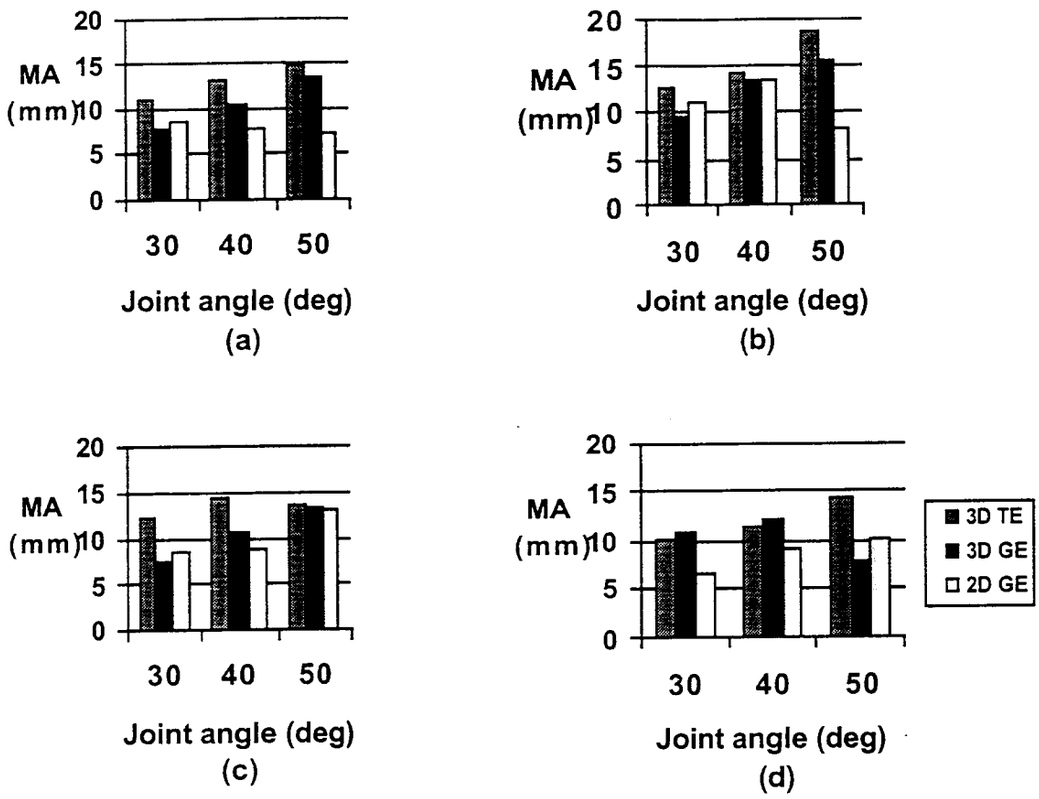

Figure 1.a.i.4. Panels (a), (b), (c), (d) contain moment arms averaged over data from the two days. Methods compared are 3D tendon excursion (3D TE), 3D geometric (3D GE), and 2D geometric (2D GE). Subjects are JK, QZ, RM, and AZ in (a), (b), (c), and (d), respectively.

Moment arms from the 3D tendon excursion and 3D geometric methods tend to be similar despite the fact that the calculations are very different. This agreement increases our confidence in the measurements. Moment arms from both the 3D tendon excursion and 3D geometric methods tend to increase as a function of flexion.

Plans for next quarter

We will continue the analysis of these data. In particular, we will examine reproducibility of the analysis of at least one data set by multiple operators. We think that this will give a measure of the effect of segmentation error. The increase in moment arm with flexion is an interesting phenomenon. From image data, we will attempt to uncover the mechanism.

In parallel, we are beginning to acquire and examine images of the wrist. We plan to extend the moment arm methods to tendons found there.

1.a.ii. PASSIVE AND ACTIVE MOMENTS

Abstract

During the past quarter, the modelling efforts regarding the characterization of the passive moment angle curves was refined. The passive moment data from each subject were simulated by a computer model that was designed to compute the passive moment as the sum of two components. One of these components has no wrist position dependency while the other component has a linear dependency wrist

position. The model allows computation of the percentage of the total passive moment that is due to the extrinsic tendons (wrist position dependent) and due to the MP joint capsule tissues (independent of wrist position). The results show that the tendons play a greater role in restricting MP extension when the wrist is extended than when it is flexed. Also, the percentage of the total passive moment due to tendons at the MP flexion limit is greatest when the wrist is flexed and least when the wrist is extended.

Purpose

The purpose of this project is to characterize the passive properties of normal and paralyzed hands. This information will be used to determine methods of improving hand grasp and hand posture in FES systems.

Report of Progress

We have previously reported on some preliminary results with a computer model which enabled us to identify the separate contributions of the extrinsic muslcle/tendon units and the tissues of the joint capsule to the total passive moment. The model computed the total passive moment as the sum of two equations. One of these equations had terms with linear relationships to wrist position, while the other equation was independent of wrist position. The moment computed by the wrist dependent equation corresponds to that portion of the total passive moment that is due to the deformation of tissues that cross the wrist as well as the MP joint. Such tissues would include the extrinsic tendons such as the extensor digitorum communis, extensor indicis, flexor digitorum profundus, and flexor digitorum superficialis. The moment computed by the equation with no wrist position dependent terms corresponds to that portion of the total passive moment that is due to tissues that do not cross the wrist but do cross the MP joint. Such tissues would be those that constitute the joint capsule as well as the ligaments.

During this quarter we have refined the model techniques and applied the model to the complete data set obtained from eight normal individuals and six paralyzed individuals. The model was refined so that it used measured data points taken directly from the measured data for each subject. Previously, the modelled moment angle curves (described in QPR#4) at each wrist angle were used as the input to the tissue contribution model.

The equation used to describe the intrinsic passive moment is:

$$M_I = K_1(e^{-K_2(\emptyset - K_3)} - 1) - K_4(e^{K_5(\emptyset - K_6)} - 1) \qquad \text{(1.a.ii.eq1)}$$

where M_I is the intrinsic passive moment in N·cm, $\emptyset$ is the MP joint angle in radians, and K_1 through K_6 are parameters defining the intrinsic moment. The part of the intrinsic passive moment defined by parameters K_1 through K_3 is produced when the MP joint extends. Thus, K_1 through K_3 describe the passive properties of the intrinsic tissues that cross the MP joint volar to the joint's axis of rotation. Parameters K_4 through K_6 describe the intrinsic moment produced when the MP joint is flexed, and therefore correspond to properties of the intrinsic tissues that lie dorsal to the axis of rotation of MP joint.

The extrinsic passive moment is defined by following equation:

$$M_E = K_7(e^{-K_8(\emptyset - (K_9 \cdot w + K_{10}))} - 1) - K_{11}(e^{K_{12}(\emptyset - (K_{13} \cdot w + K_{14}))} - 1) \qquad \text{(1.a.ii.eq2)}$$

where M_E is the extrinsic passive moment in N·cm, $\emptyset$ is the MP joint angle in radians, w is the wrist position in degrees, and K_7 through K_{14} are parameters defining the extrinsic moment. The part of the extrinsic passive moment described by parameters K_7 through K_{10} is produced when the MP joint extends. This corresponds to the passive moment produced by extrinsic tissues that lie volar to the axis of rotation of the MP joint. These tissues include the muscle/tendon units of the FDS and FDP. Conversely, parameters K_{11} through K_{14} describe the extrinsic moment produced when the MP joint is flexed. This part of extrinsic passive moment is produced by tissues that cross the MP joint dorsal to its axis of rotation and include the EDC and EI.

The total passive moment is the sum of the previous two moments:

$$M_{Total} = M_I + M_E \qquad \text{(1.a.ii.eq3)}$$

where M_{Total} is the total passive moment. Equation 2.4 was expressed as an objective function and its implicit 14 parameters (K_1 through K_{14}) were computed using the Levenberg-Marquardt algorithm for solving nonlinear systems of equations. Once the 14 parameters were computed for each subject, the separate intrinsic and extrinsic moments could be computed as a function of wrist position and MP joint angle using Equations 1.a.ii.eq1 and 1.a.ii.eq2.

The data required as input to the parameter estimation algorithm were moment-angle data points from the original MACs recorded for each wrist position. Fifty-nine data points evenly spaced between the flexion and extension extremes (defined by the limit switches) were extracted from each of a given subject's seven MACs. This made a total of 413 data points as input to the parameter estimation algorithm for each subject. Therefore, the algorithm computed a best fit for the 14 unknowns in 413 nonlinear equations.

Modified Model Results

The output of the model, after it is applied to all seven curves measured from a single subject, is a set of eight curves, as shown in Figure 1.a.ii.1. One curve describes the contribution of the intrinsic tissues as a function of MP angle. The remaining seven curves describe the contribution of the tendon/muscle units at each of the seven wrist angles. The model allows the extensor muscles to have a different dependency on wrist angle than the flexor muscles. For the subject data shown in Figure 1.a.ii.1, the extension side of the extrinsic moment shifts more per change in wrist position than the flexion side of the extrinsic moment. Typically, the curve for the intrinsic tissues shows that these tissues are stiffer than the muscle/tendon units.

An example of the model's fit of the total passive moment for a single able bodied subject at all seven wrist positions is shown in Figure 1.a.ii.2. Each subplot of this figure corresponds to a different wrist position. Two traces are shown in each subplot. The small filled circles are moment-angle data points extracted from the original MACs. These data were the input to the model. The solid trace is the model's simulation of the input data; it is the sum of intrinsic and extrinsic components. Note that all the passive moments determined by the model were computed from a single set of 14 parameters, indicating that the model captures the dependence of moment on both wrist and MP joint angles. For this subject, 93% of the total variance in the data was accounted for by the model. Across all subjects, the model accounted for between 90% and 94% of the total variance in the data. Table 1.a.ii.1 lists the median of each parameter of Equations 1.a.ii.eq1 and 1.a.ii.eq2 from the able bodied subject population.

Table 1.a.ii.1. Median of Parameters K_1 through K_{14} for Able Bodied Subjects

Parameter	*Median*
K_1 (N·cm)	1.3
K_2 (rad^{-1})	3.9
K_3 (deg)	-18.0
K_4 (N·cm)	1.6
K_5 (rad^{-1})	5.3
K_6 (deg)	79.4
K_7 (N·cm)	1.1
K_8 (rad^{-1})	2.4
K_9 (none)	-0.7
K_{10} (deg)	10.9
K_{11} (N·cm)	0.8
K_{12} (rad^{-1})	3.1
K_{13} (none)	-0.3
K_{14} (deg)	40.8

Figure 1.a.ii.3 shows the separate components of the total passive moment for this same subject at two wrist positions. The small filled circles and solid trace in each subplot are the same as those in Figure 1.a.ii.2. The thick gray trace in Figure 1.a.ii.3 is the intrinsic passive moment, and the thin black trace is the extrinsic passive moment. These are the same curves as those shown in Figure 1.a.ii.1. Figure 1.a.ii.3 shows that when this subject's wrist was extended 60°, the passive moment during MP joint extension was produced by the extrinsic muscle/tendon units, but when the MP joint was flexed, the passive moment was generated almost entirely by the intrinsic tissues localized to the joint. The opposite tissues restrained the ranges of motion when the wrist was flexed 60°. At wrist positions in between the two extremes, the extrinsic moment and intrinsic moment added together in changing proportions to generate the total passive moment at the limits of MP flexion and extension.

For each subject the percentage of the total passive moment produced by the extrinsic tissues at the flexion and extension limits were computed for each wrist position. The medians of these percentages for both subject populations are shown in Figure 1.a.ii.4 by the two traces. The top plot shows the percentage of the total passive moment produced by the flexor muscles at the MP joint's extension limit. The bottom plot shows

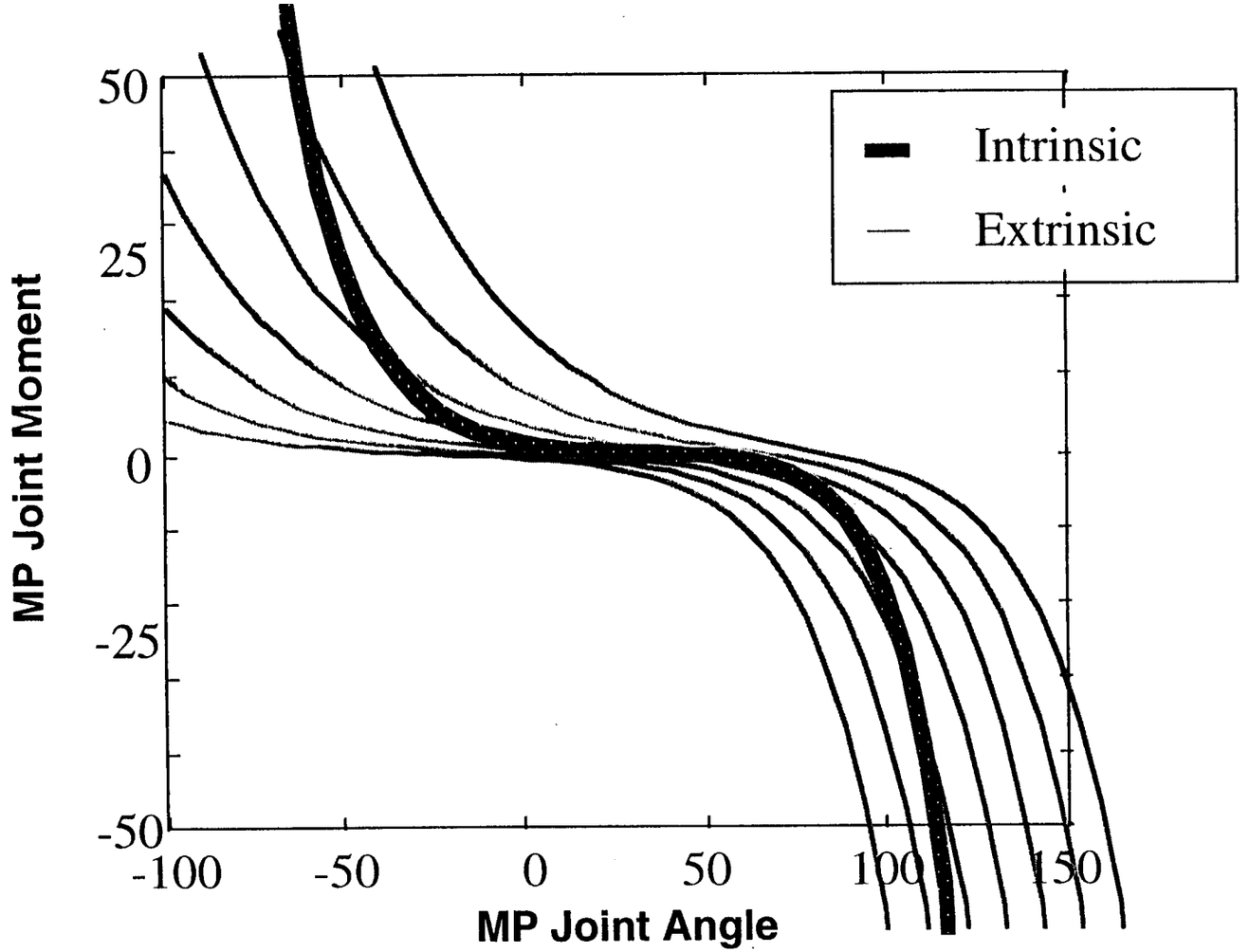

Figure 1.a.ii.1. Example for one subject of the calculated contributions of the extrinsic and intrinsic tissue. The multiple extrinsic curves show the contributions at the seven different wrist angles. There is a separate gain for the extensor and flexor tendon/muscle groups.

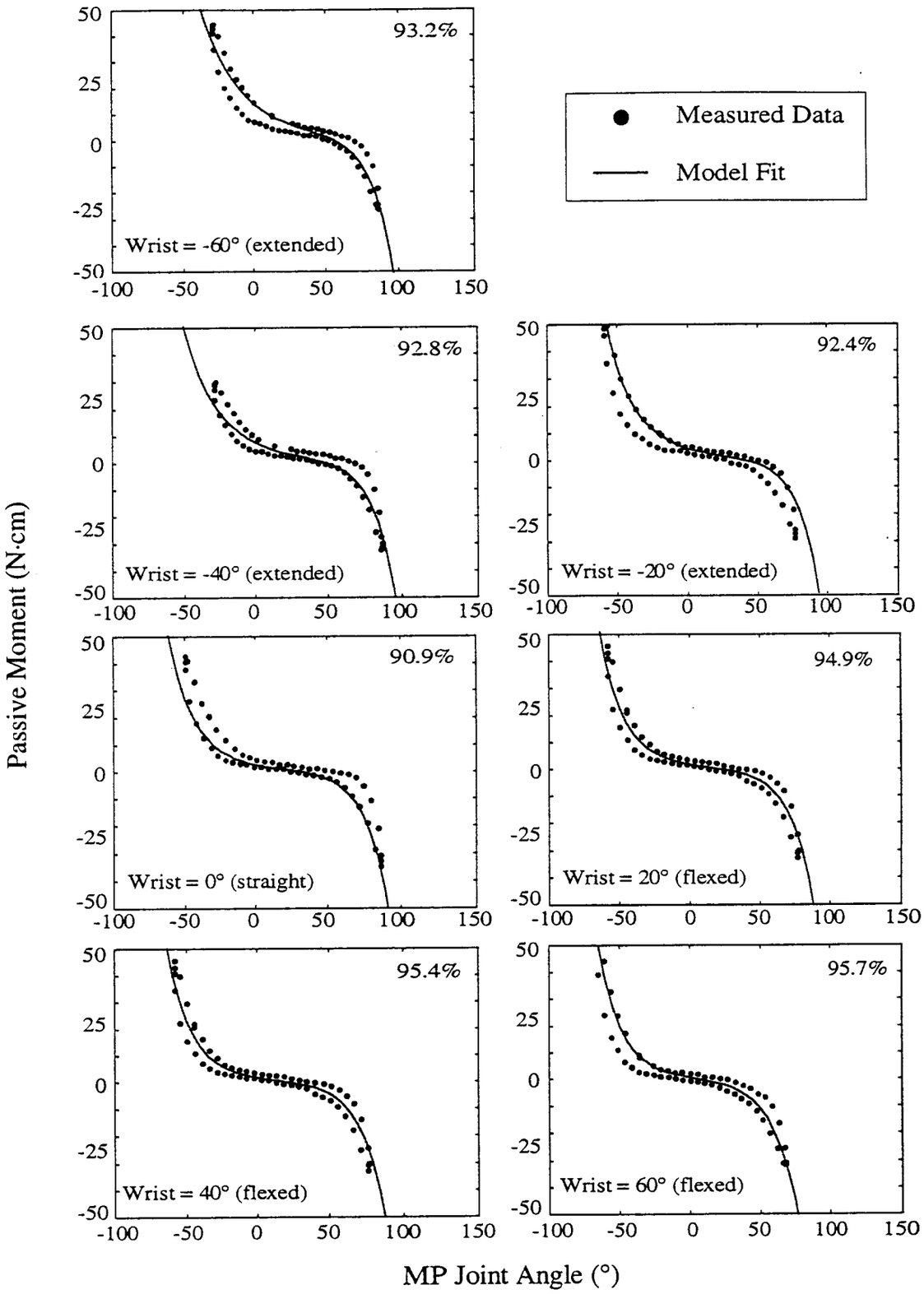

Figure 1.a.ii.2. Model fit to measured data for one able bodied subject at all seven wrist positions. The variance in the data accounted for by the model is shown in the upper right hand corner of each subplot.

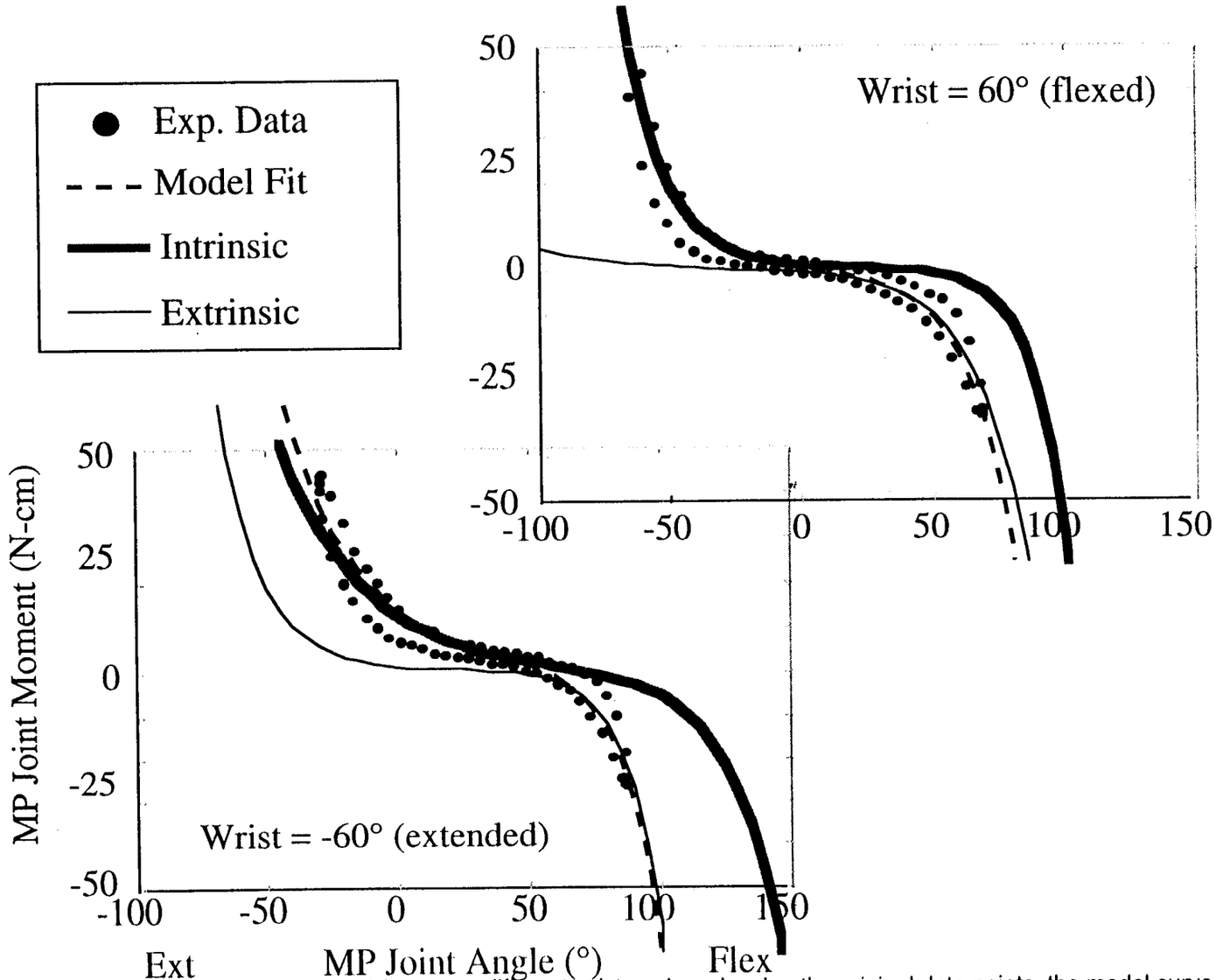

Figure 1.a.ii.3. Example of the model fits at two different wrist angles, showing the original data points, the model curve fit, and the estimated contributions of the extrinsic and intrinsic tissues.

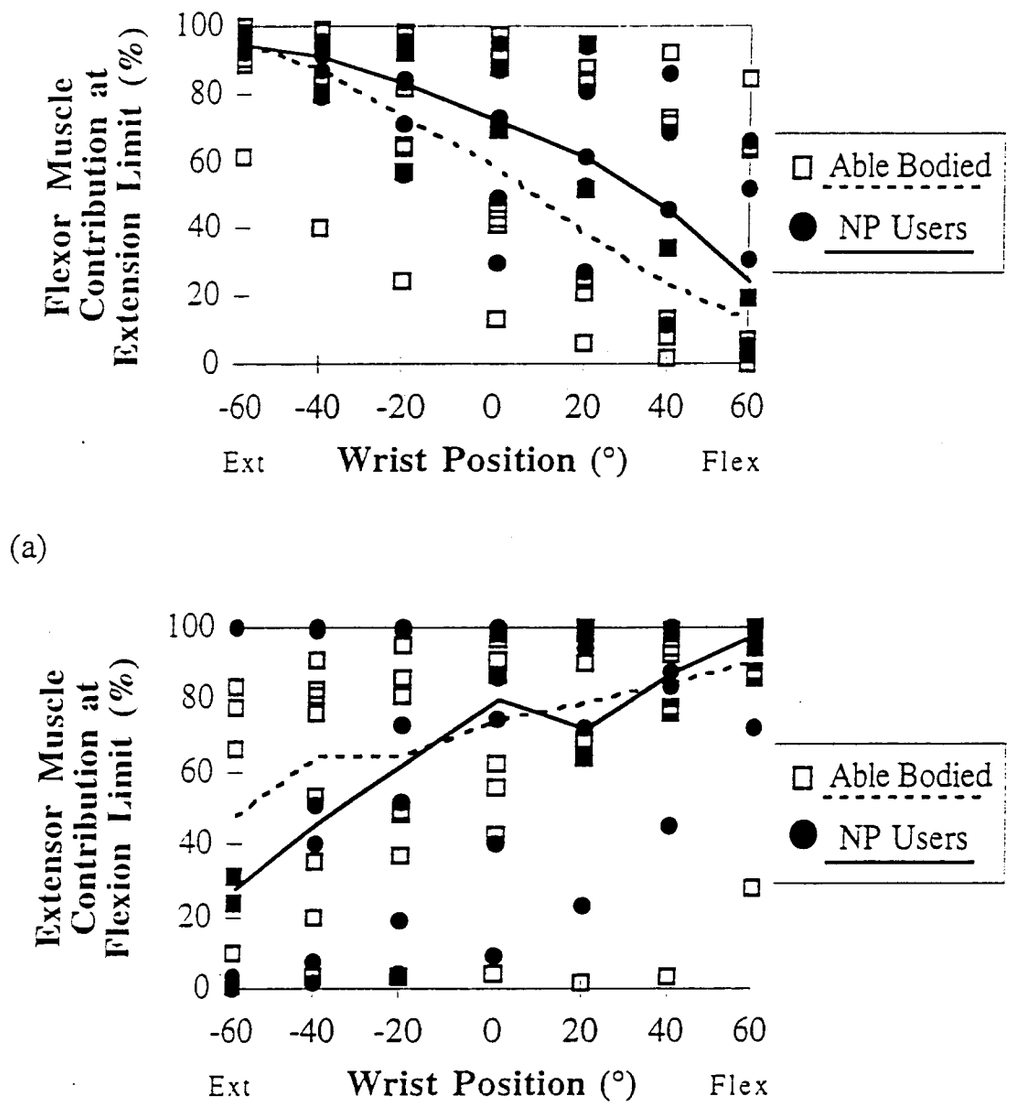

Figure 1.a.ii.4. Extrinsic muscle contributions to the total passive moment at the MP joint for the extension limit (top graph) and the flexion limit (bottom graph). Data for each subject are included. The medians for both populations are indicated by the solid and dotted traces.

the percentage of the total passive moment produced by the extensor muscles at the MP joint's flexion limit. Each subject's percentage was plotted in these figures to show the wide range of percentages across the population.

The medians show that the flexor muscles of both populations accounted for about 90% of the total moment at the MP joint's extension limit when the wrist was extended 60°. The remaining 10% was generated by the intrinsic tissues. When the wrist was flexed 60° the flexor muscles contributed only about 15% to 25% of the passive moment at the extension limit and the intrinsic tissues were largely responsible for restraining MP joint extension in both populations. In general, the flexor muscles' contribution to the total passive moment at MP extension decreased as the wrist was fixed in positions from 60° of extension to 60° of flexion. The opposite effects occurred at the MP joint's flexion limit. Comparing the medians for the flexors and extensors shows that the flexor muscles are more wrist-dependent than the extensor muscles.

There was no significant difference between the two populations in how the extrinsic muscles contribute to the passive moment at the extension and flexion limits. However, Figure 1.a.ii.4 does indicate that there were wide ranges of data for both populations at each wrist position.

For all subjects but one the flexor muscles were found to produce over 85% of the total passive moment when the MP joint was at its extension limit with the wrist extended 60°. Likewise, in 12 of the 14 subjects, the extensor muscles contributed over 85% of the total passive moment when the MP joint was at its flexion limit while the wrist was fixed at 60° of flexion.

Plans for Next Quarter

During the next quarter, the information derived from the passive moment model will be incorporated into the biomechanical model of the hand. We will also begin to look at methods for making measurements of the passive properties of the distal joints of the fingers.

1. b. BIOMECHANICAL MODELING: ANALYSIS AND IMPROVEMENT OF GRASP OUTPUT

Abstract

Individual muscle function in tetraplegics differs substantially from able-bodied persons due to factors such as decreased joint range of motion, muscle contractures, surgically altered muscle lines of actions, and adhesions. In order to evaluate and improve hand grasp in neuroprosthesis users, we are developing biomechanical models of the upper extremity that more accurately reflect muscle strengths and actions in tetraplegics. These models will be used to analyze the biomechanical sources of shortcomings in neuroprosthetic hand function and to design procedures to enhance function. During this quarter, we have developed a preliminary model of the brachioradialis to extensor carpi radialis brevis tendon transfer and we have obtained measurements of isometric elbow and shoulder moment-angle curves in tetraplegic subjects. In the future, the measurement methods described in this report will be used to test and validate our current model of the tendon transfer.

Objective

The purpose of this project is to use the biomechanical model and the parameters measured for individual neuroprosthesis users to analyze and refine their neuroprosthetic grasp patterns.

Report of Progress

We have initiated projects to quantify moment-generation and muscle function in neuroprosthesis users and to incorporate these findings into a biomechanical model of the elbow and wrist. During this quarter we (i) developed a moment transducer to measure the elbow flexion-extension moments generated via functional electrical stimulation or voluntary contraction in neuroprosthetic users, (ii) combined measurements of the forces and moments generated at the shoulder and elbow during stimulation of the biceps to quantify variations in force and moment arm as a function of elbow flexion angle in one tetraplegic subject, and (iii) developed a preliminary model of the brachioradialis to extensor carpi radialis brevis tendon transfer (Br-ECRB transfer).

Elbow Moment Transducer

A moment transducer has been developed to measure the elbow flexion-extension moments generated via functional electrical stimulation or voluntary contraction in tetraplegic subjects. The elbow moment transducer is based on an individual linkage of the finger moment transducer (described in previous progress reports), scaled in size to fit the elbow joint. The transducer is a system of two four-bar linkages, held together by a joint whose position can be adjusted and locked to allow measurements of isometric flexion-extension moments at different elbow flexion angles. Two strain gauges are attached to the base of one of the supports of the system, and the device is bolted to a Bledsoe brace, which is used to mount the device on the subject's upper arm and forearm. The voltage output (V) from the transducer is converted into a moment (Nm) using a linear calibration curve that was determined by applying known moments to the transducer under simulated experimental conditions (Fig. 1.b.1A). Calibration data was collected using a Delrin "arm", made from two Delrin beams connected by a hinge joint. The Delrin arm was secured to the Bledsoe brace and moment transducer, and extension moments were applied to the transducer by loading the delrin arm with a known mass at a distance of 0.284 m from the hinge joint. Calibration data for extension moments was collected with the transducer positioned in different flexion positions and in two orientations: horizontal, simulating measurements with the shoulder abducted, and vertical, simulating measurements with the

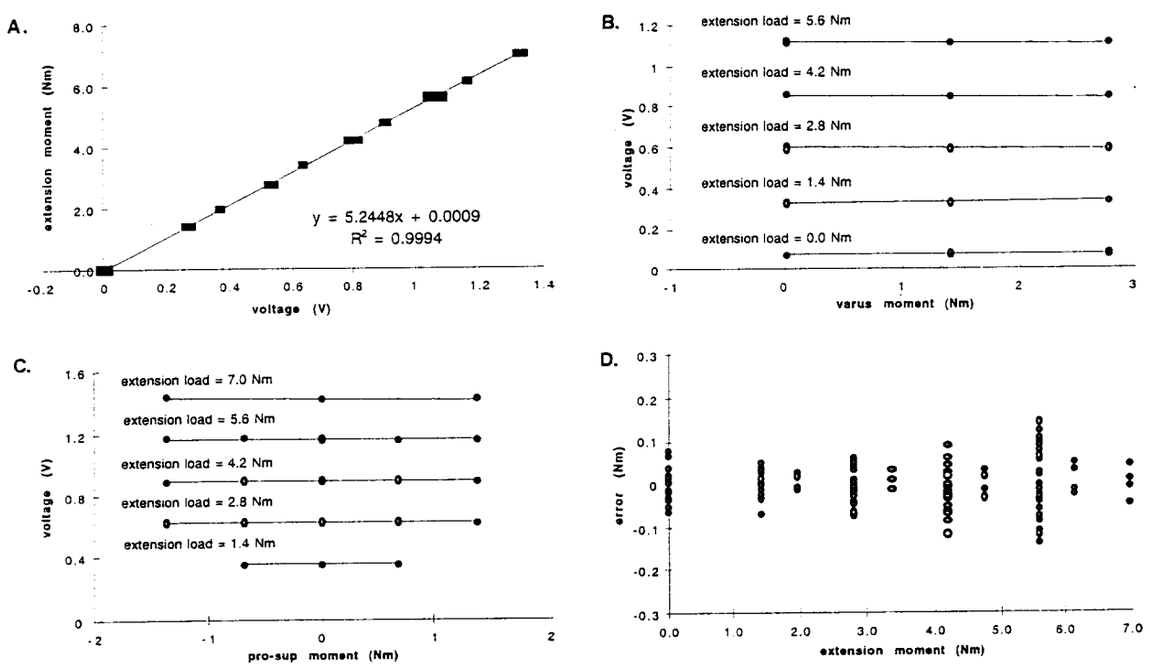

Figure 1.b.1 (A). Linear regression between applied extension moment and output voltage of the elbow moment transducer. Calibration data was collected in varying positions and orientations, as well as in the presence of substantial off-axis loads. The slope of the regression fit (5.2448 Nm/V) is the calculated gain of the transducer. (B). Output voltage of the transducer as a function of applied varus loads. The effect of varus loads on transducer output was minimal at all five extension loads tested. (C). Output voltage of the transducer as a function of applied pronation-supination loads. The effect of pronation-supination loads on transducer output was minimal at all of the extension loads tested. (D). Residuals between the extension moment estimated using the linear regression fit and the applied extension moment. The transducer estimates the applied moment to within 0.2 Nm, even in the presence of substantial off-axis loads.

shoulder adducted. Also, calibration data was collected in the presence of varus-valgus (Fig. 1.b.1B) and pronation-supination loads (Fig. 1.b.1C) to evaluate the effects of off-axis moments on the voltage output of the transducer. The gain of the transducer (5.2448 Nm/V) was estimated using all of the calibration data points. The calibration data from separate trials were first combined by subtracting the measured offset

(voltage output at 0 Nm load) for a given trial from all of the voltage readings for that trial. The slope of the extension moment vs. voltage curve was then estimated using linear regression analysis. An error analysis was performed by evaluating the residuals between the linear fit and the applied moment (Fig. 1.b.1D). Using the gain estimated from the linear regression, the transducer estimates the applied extension moment to within 0.2 Nm over the tested range of 0 Nm to 7.0 Nm, even in the presence of substantial off-axis loads. Presently, we are in the process of calibrating the device for measurement of elbow flexion moments. In addition, we are verifying the device's performance on subjects by comparing moment-angle curves measured with the transducer to moment-angle curves measured using a six-axis force-moment transducer.

Estimating Moment Arms and Force-Angle Curves from Two-Joint Muscles

We have measured the forces and moments generated about the shoulder and elbow simultaneously, as a function of elbow flexion angle, during percutaneous stimulation of the biceps and triceps in a C3 tetraplegic subject (Fig. 1.b.2A and 1.b.2B). The subject was seated in his wheelchair, positioned in front of a table. His forearm was casted and the fiberglass cast was bolted to an aluminum beam attached to a six-axis force-moment transducer (JR3, Inc.), which was mounted on a pedestal that could be secured to the tabletop. The subject's shoulder was abducted, and positioned in 0° horizontal flexion, and his forearm was placed in the cast attached to the transducer. During the measurement protocol, elbow position was varied from 20° to 90° flexion in 10° increments (0° is full extension) by re-positioning the transducer on the table. In each trial, the subject's biceps or triceps was stimulated via a percutaneous electrode, and the resulting forces and moments measured by the transducer were sampled at 25 Hz. The measured forces and moments were referenced to the approximate centers of rotation of the elbow and shoulder using a homogeneous transformation based on the elbow and shoulder positions, and the measured distances between the center of the JR3 transducer, the lateral epicondyle of the humerus, and the acromion landmark of the scapula. Given this transformation, we measured the elbow flexion-extension and varus-valgus moments, forearm pronation-supination moment, shoulder horizontal flexion, abduction-adduction, and internal-external rotation moments generated by the biceps and triceps during functional electrical stimulation.

Because the biceps crosses both the shoulder and elbow, the measured shoulder and elbow moments were also used to estimate the variation in biceps elbow flexion moment arm and force as a function of elbow flexion angle. Specifically,

$$M_e = r_e * F \qquad (1)$$

$$M_s = r_s * F \qquad (2)$$

where F is the force developed by the biceps, M_e and M_s are the magnitudes of the flexion moments generated about the elbow and shoulder, respectively, and r_e and r_s are the flexion moment arms about the elbow and shoulder, respectively. Thus,

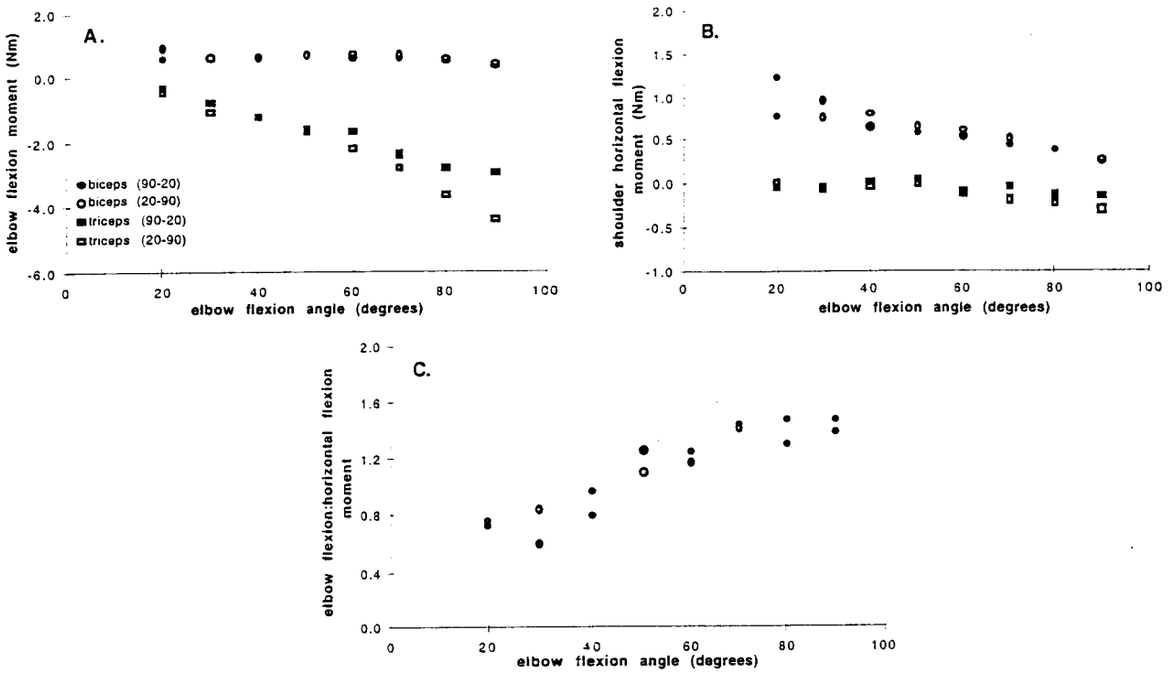

Figure 1.b.2 (A). Isometric elbow flexion moment generated by the biceps and triceps during functional electrical stimulation as a function of elbow flexion angle. Positive indicates flexion, negative indicates extension. 0° is full extension. The magnitude of the triceps extension moment varies substantially with elbow position and was larger than the biceps flexion moment in flexed elbow positions. (B). Isometric horizontal flexion moment generated at the shoulder during function electrical stimulation by the biceps and triceps during functional electrical stimulation. Positive indicates horizontal flexion. The horizontal flexion moment generated by the biceps varies as function elbow flexion angle. Because the shoulder position was kept constant throughout the protocol, variation in the measured shoulder flexion moment indicates the variation in muscle force developed by the biceps at different elbow flexion angles. The triceps did not generate a flexion moment at the shoulder, probably because we were stimulating the medial or lateral head, which do not cross the shoulder joint. (C). The ratio of elbow flexion moment to horizontal flexion moment generated by the biceps. This ratio provides an estimate of the magnitude of the biceps elbow flexion moment arm relative to the shoulder flexion moment arm, and illustrates the variation in elbow flexion moment arm as a function of elbow flexion angle.

$$\frac{M_e}{M_s} = \frac{r_e}{r_s} \qquad (3)$$

Because shoulder position was kept constant (while elbow position was varied), the moment arm at the shoulder is constant across trials. As a result, differences in the ratio of the measured elbow flexion moment to shoulder horizontal flexion moment at different elbow flexion angles indicate the variation in elbow flexion moment arm that occurs with elbow flexion angle (Fig. 2C). Similarly, because shoulder position was kept constant, the variation in the moment generated at the shoulder joint in different trials reflects the variation in force developed by the biceps at different elbow flexion angles (Eq. 2, Fig. 1.b.2B).This method will be implemented in the future to quantify the variation in moment arm and muscle force as a function of joint position in two-joint muscles across a number of different subjects, providing valuable information for the development of biomechanical models that represent spinal cord injured subjects.

Biomechanical Model of Br-ECRB tendon transfer

We have developed a preliminary model of the brachioradialis to extensor carpi radialis brevis tendon transfer that is commonly performed in tetraplegic patients who receive implanted neuroprosthetic systems. The model was developed using the Software for Interactive Musculoskeletal Modeling (SIMM, Musculographics, Inc.) and includes three-dimensional surface representations of the bones of the arm, forearm, and hand, kinematics of the elbow and wrist, and force-generating properties of the brachioradialis and ECRB. The bones of the humerus, radius, ulna, carpal bones, and hand bones are defined by polyhedra that describe the bone surfaces. The elbow joint is defined by a homogeneous transformation from the humeral reference frame to the ulnar reference frame. Elbow flexion/extension is represented as a uniaxial hinge joint, with its axis passing through the centers of the capitulum and the trochlear sulcus. Elbow flexion is modeled from full extension (defined as 0° flexion) to 130° flexion. Currently, the wrist kinematics are constrained to planar wrist flexion-extension, with wrist motion distributed evenly over the radiocarpal and midcarpal rows. The axes of rotation in the model are located near the center of the lunate for the radiocarpal joint, and near the center of the capitate for the midcarpal joint. Wrist flexion is modeled from 70° extension to 70° flexion. The wrist model was obtained from Northwestern University, and has been described previously (Gonzalez *et al.*, 1997).

Muscle-tendon paths for the brachioradialis and extensor carpi radialis brevis were defined based on the anatomical landmarks of the three-dimensional bone models and using digitized muscle attachment sites and muscle paths from a previous study (Murray, 1997). Muscle-tendon paths vary as a function of joint angle, and the modeling software calculates the lengths of the paths as a function of both elbow and wrist position. Moment arms (*ma*) are computed as the partial derivative of muscle-tendon length, $\partial \ell$, with respect to joint angle, $\partial \theta$. That is,

$$ma = \frac{\partial \ell}{\partial \theta} \qquad (4)$$

The isometric force-generating properties of the brachioradialis and ECRB were derived by scaling generic active and passive force-length curves for muscle and tendon by four parameters: peak isometric force (F_o^M), optimal muscle fiber length (ℓ_o^M), pennation angle (α), and tendon slack length (ℓ_s^T). Estimates of F_o^M, ℓ_o^M, and α were derived from detailed anatomical measurements of muscle architectural parameters (see Murray, 1997 and Gonzalez *et al.*, 1997 for summary). Tendon slack length for ECRB was taken from the model developed by Gonzalez *et al.* Tendon slack length for brachioradialis was defined so that the isometric force developed by Br during full activation varied as a function of elbow flexion angle according to the biomechanical analysis described in Murray (1997).

The muscle-tendon path that models the Br-ECRB tendon transfer is a hybrid of the brachioradialis and ECRB paths described above. At the elbow joint, the transfer path is identical to the path of brachioradialis; therefore, the modeled transfer has the same elbow flexion moment arm as the brachioradialis. Similarly, at the wrist joint, the transfer's path and wrist extension moment arm are identical to ECRB. The transfer's muscle-tendon path along the forearm is based on comments from a hand surgeon regarding the location of the surgical incision on the forearm and the degree the brachioradialis is released from its surrounding fascia during surgery. Three of the four force-generating parameters of the transfer (F_o^M, ℓ_o^M, and α) are identical to brachioradialis. Tendon slack length of the transfer was adjusted so that the force-generating capacity of the transfer as a function of elbow flexion angle was similar to the force-generating capacity of the brachioradialis path.

Our preliminary model of the Br-ECRB tendon transfer indicates that the maximum isometric wrist extension moment developed by the transfer is dependent on elbow flexion angle (Fig. 1.B.3). This effect could potentially limit a neuroprosthesis user's ability to position the hand in tasks where the elbow is flexed, such as eating or grooming. Weakness in the Br-ECRB transfer with elbow flexion has been discussed anecdotally in surgical texts (see Brand, 1985) and has been observed clinically in some neuroprosthesis users. We plan to further investigate the dependence of wrist extension strength on elbow flexion after transfer of the brachioradialis to ECRB by quantifying wrist extension moment-angle curves in transfer patients in different elbow positions. Because the transferred muscle crosses both the wrist and

elbow, we will also estimate the variation in moment arm and muscle force developed by the transferred muscle in order to further validate our biomechanical model.

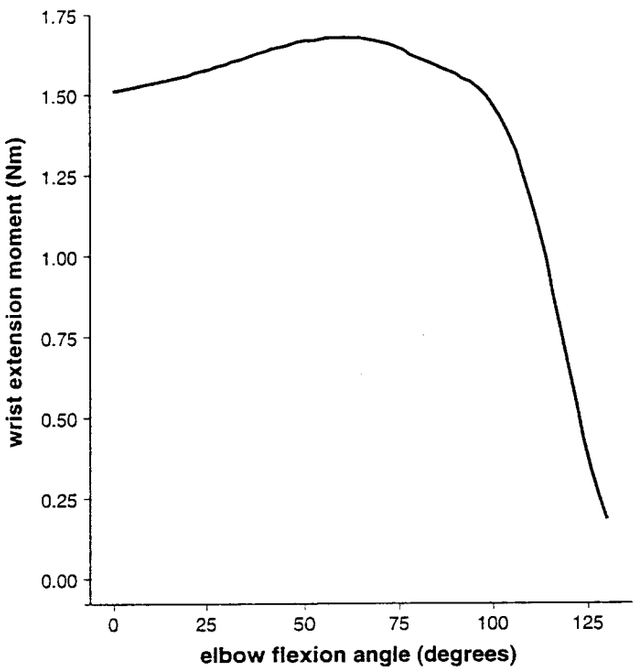

Figure 1.B.3. Isometric wrist extension moment generated at 0° wrist flexion by the Br-ECRB transfer model as a function of elbow flexion angle. 0° elbow flexion is full elbow extension. Our model indicates that the wrist extension moment generated by the transfer decreases substantially in flexed elbow positions, potentially limiting the ability to position the hand in tasks where the elbow is flexed.

Plans for Next Quarter

In the next quarter, we plan to further investigate and model the Br-ECRB transfer. Clinically, we will contact tetraplegic subjects who have undergone the transfer and enroll them in a study to quantify the effects of elbow position on the wrist extension moment generated by the transfer. We will continue development of the elbow moment transducer and evaluate its performance when loaded with flexion moments. In addition, we will investigate if the elbow moment transducer can be used in series with a wrist moment transducer to simultaneously measure the elbow flexion and wrist extension moments generated by the Br-ECRB transfer. Continued development of the biomechanical model will include (i) digitizing the transfer in an anatomical specimen, (ii) modeling triceps muscle function to balance the elbow flexion moment generated by the brachioradialis during wrist extension, (iii) modeling the passive muscle properties of the wrist flexors in tetraplegic subjects, and (iv) adding dynamics to model.

References

Brand, P. W. (1985) Clinical Mechanics of the Hand. The C. V. Mosby Company, St. Louis.

Gonzalez, R. V., Buchanan, T. S. and Delp, S. L. (1997) How muscle architecture and moment arms affect wrist flexion-extension moments. *J Biomech* 30:705-712.

Murray, W. M. (1997) The functional capacity of the elbow muscles: anatomical measurements, computer modeling, and anthropometric scaling. Ph.D. Dissertation, Northwestern University, Evanston, IL.

2. CONTROL OF UPPER EXTREMITY FUNCTION

Our goal in the five projects in this section is to either assess the utility of or test the feasibility of enhancements to the control strategies and algorithms used presently in the CWRU hand neuroprosthesis. Specifically, we will: (1) determine whether a portable system providing sensory feedback and closed-loop control, albeit with awkward sensors, is viable and beneficial outside of the laboratory, (2) determine whether sensory feedback of grasp force or finger span benefits performance in the presence of natural visual cues, (of particular interest will be the ability of subjects to control their grasp output in the presence of trial-to-trial variations normally associated with grasping objects, and in the presence of longer-term variations such as fatigue), (3) demonstrate the viability and utility of improved command-control algorithms designed to take advantage of forthcoming availability of afferent, cortical or electromyographic signals, (4) demonstrate the feasibility of bimanual neuroprostheses, and (5) integrate the control of wrist position with hand grasp.

2. a. HOME EVALUATION OF CLOSED-LOOP CONTROL AND SENSORY FEEDBACK

Abstract

The purpose of this project is to deploy an existing portable hand grasp neuroprosthesis capable of providing closed-loop control and sensory feedback outside of the laboratory. Work this quarter was restricted to repair of the power management circuitry of the original portable closed loop system unit.

Purpose

The purpose of this project is to deploy an existing portable hand grasp neuroprosthesis capable of providing closed-loop control and sensory feedback outside of the laboratory. The device is an augmented version of the CWRU hand neuroprosthesis, and was developed and fabricated in the previous contract period. The device utilizes joint angle and force sensors mounted on a glove to provide sensory information, and requires daily support from a field engineer to don and tune. The portable feedback system is not intended as a long term clinical device. Our goal, rather, is to evaluate whether the additional functions provided by this system benefit hand grasp outside of the laboratory, albeit with poor cosmesis and high demands for field support.

Report of Progress

Two portable closed-loop control systems (PCLS) have been built previously, but one had been shelved due to problems in the power supply and power management circuitry. However, that unit had to be repaired because the laboratory investigation on the effects of sensory feedback in the presence of vision now uses a PCLS also making two units necessary.

Plans for Next Quarter

The PCLS repairs will be completed, and subject *L* (see previous report) will be asked to participate in home evaluations.

2. b. INNOVATIVE METHODS OF CONTROL AND SENSORY FEEDBACK

2. b. i. ASSESSMENT OF SENSORY FEEDBACK IN THE PRESENCE OF VISION

Abstract

The purpose of this project is to develop a method for including realistic visual information while presenting other feedback information simultaneously, and to assess the impact of feedback on grasp performance in the presence of such visual information. In this quarter, the video acquisition system was completed, including preliminary tests of the evaluation protocol. Those tests revealed an erratic appearance of the video playback in steep segments of the recruitment curve. Methods are being developed

to alter the video frame density over those regions while reducing the density in regions where the output force is independent of command.

Purpose

The purpose of this project is to develop a method for including realistic visual information while presenting other feedback information simultaneously, and to assess the impact of feedback on grasp performance. Vision may supply enough sensory information to obviate the need for supplemental proprioceptive information via electrocutaneous stimulation. Therefore, it is essential to quantify the relative contributions of both sources of information.

Report of Progress

The video simulation system was implemented and tested in its entirety. In these preliminary tests, an able-bodied subject donned a shoulder controller and used it to control a video clip, generating both motion of the hand on the video display as well as a commensurate force signal for controlling sensory feedback and for input to the acquire & hold test software. The subject was able to complete the acquire & hold task exactly as it is performed in the PCLS evaluations described previously. However, it became apparent that the video display was erratic in certain regions of the command range where force increased rapidly for a small change in command.

An example of such a recruitment function is shown by the solid line in Fig. 2.b.1, the average of ten recruitment functions recorded with the sigmoidal command ramp described previously. The force increases sharply at 60% command, the onset of stimulation of the thumb flexors for this neuroprosthesis user. Clearly it will be necessary to "sample" this region more densely when recording the video clip so that each frame corresponds to a smaller command increment to keep the change in force per frame within acceptable limits. The dashed line in Fig. 2.b.1 shows a nominal recruitment function, also starting at 60% command. (Recall that the command range is divided up into three regions: an initial deadband that insures that the hand opens fully initially, followed by a range over which the thumb is flexed without an opposing load to close the grasp, and then followed by a range in which force increases with the hand closed). It is not our purpose to alter the command map so that force is recruited smoothly over the entire command range since that would not represent typical operation of the neuroprosthesis. Rather, we simply need to ensure smooth progression of the visual image throughout the command range. Since the frame rate cannot be changed readily (it is most convenient to maintain the standard 30Hz rate), we will need to adjust the command ramp used while recording the video clip so that the command velocity is reduced in regions where the recruitment function is steep. The process is illustrated in Fig. 2.b.2 which plots the derivative of the force versus the command for both the actual (solid) and nominal (dashed) recruitment functions. If the nominal command ramp is linear so that the command is increased at a constant rate over time, then the command axis is commensurate with time. Over the range of 60-100% command, then, we need to limit the size of the command step per sample so that the resultant force increment does not exceed the increment expected for nominal recruitment. At the same time, the number of samples taken in that region will increase so that the same total command range is covered.

There are several methods to implement such sampling. The easiest numerically is to simply invert the derivatives in Fig. 2.b.2 subject to certain limits (for example, we will not use an infinite frame rate in the region where the recruitment function is flat) and use the results in a look-up table in the video collection software. That software is not designed to accept such a table, however, and it will be more efficient to fit an analytic function to the command rate data even if some detail is lost.

Plans for Next Quarter

We will implement the revised video recording scheme and collect new video clips from neuroprosthesis users. If the new command ramp algorithm is successful, we will commence our investigations of the effects of feedback in the presence of vision.

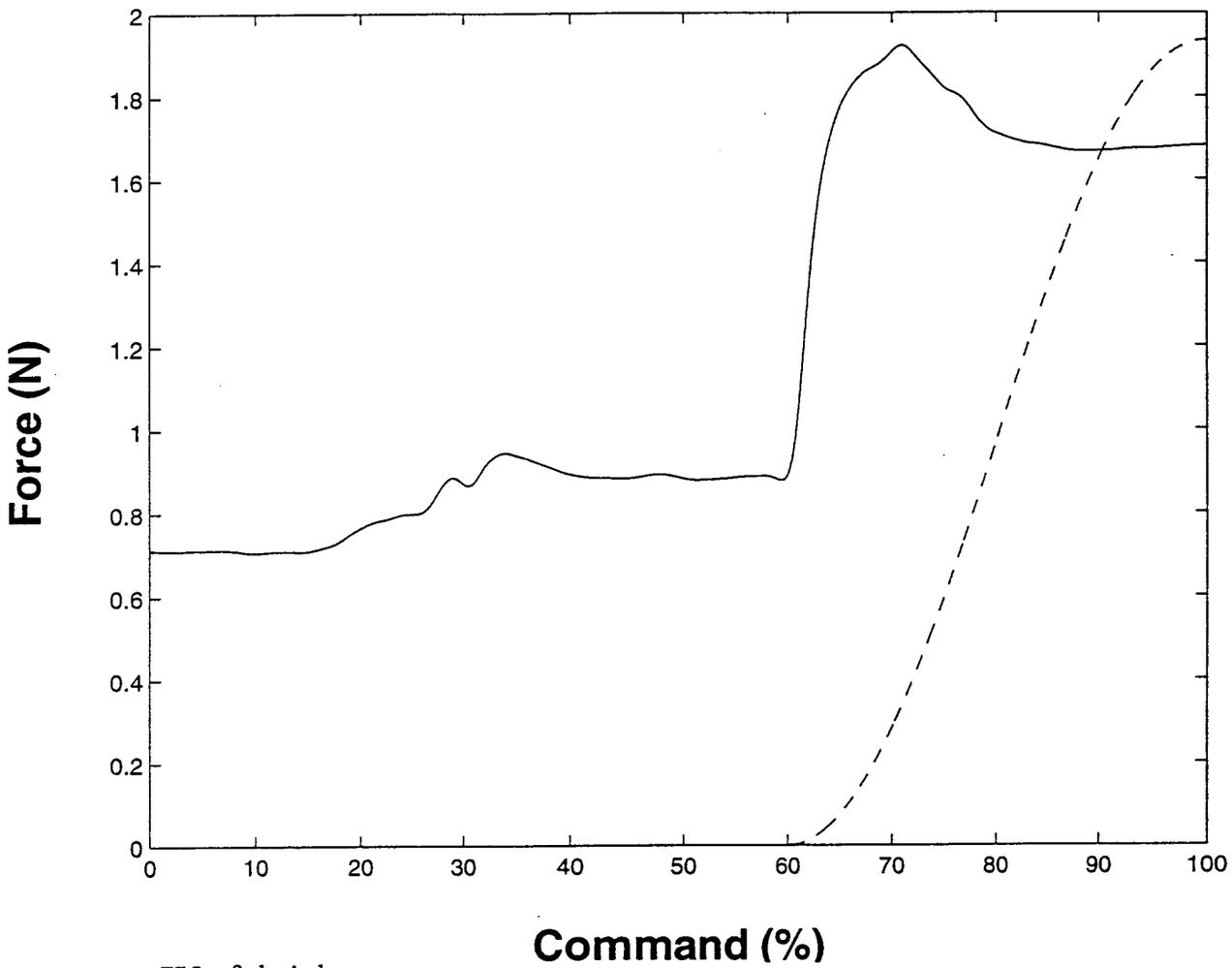
Force (N)
2
1.8
1.6
1.4
1.2
1
0.8
0.6
0.4
0.2
0
0
10
20
30
40
50
60
70
80
90
100
Command (%)

FIG. 2.b.i.1

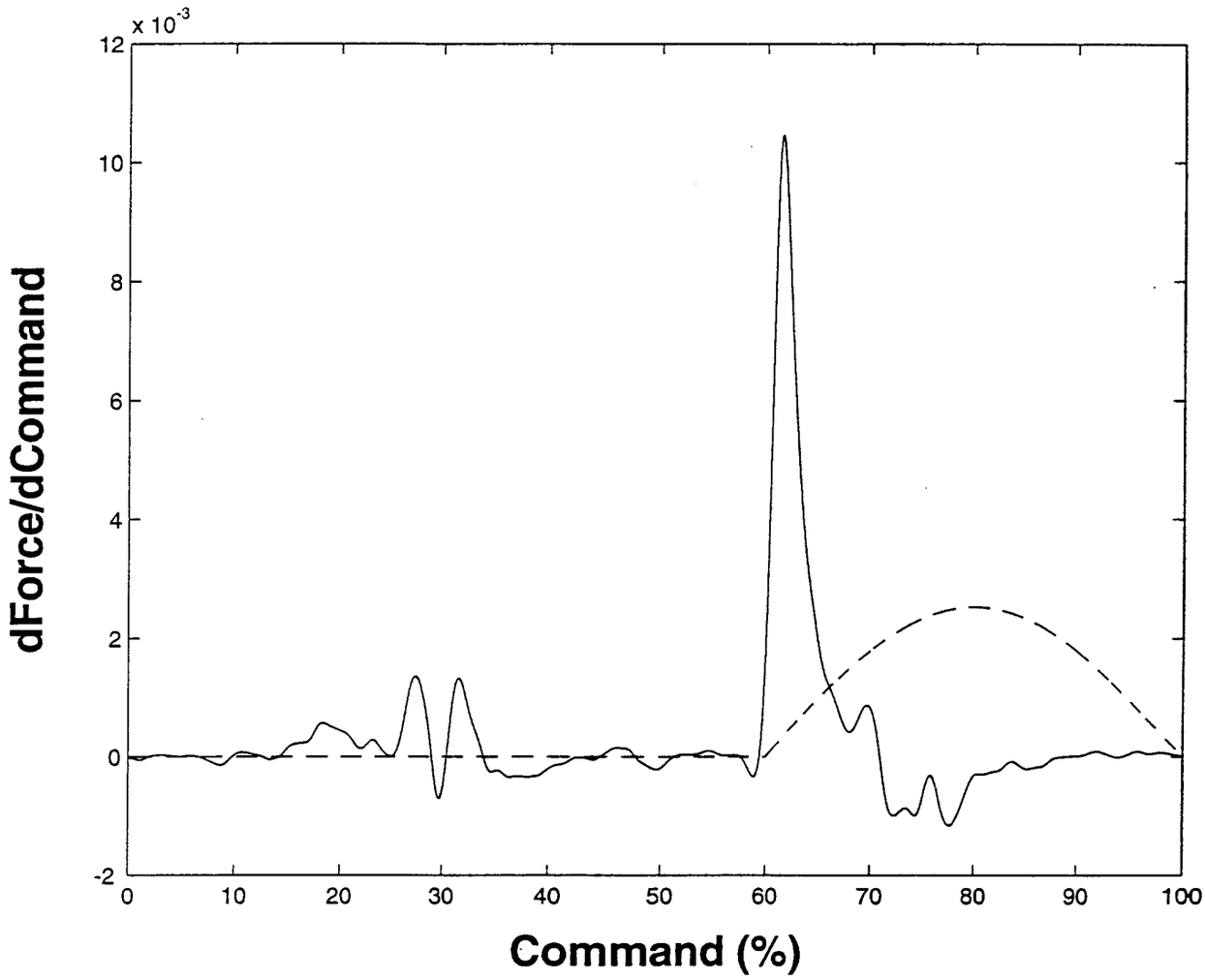
x 10^-3
12
10
8
6
4
2
0
-2
0
10
20
30
40
50
60
70
80
90
100
dForce/dCommand
Command (%)

FIG. 2.b.i.2

2. b. ii. INNOVATIVE METHODS OF COMMAND CONTROL

Abstract

During this quarter we continued analysis of the performance of a 2-element strain gage mounted on the thumbnail as a grasp force sensor and a contact sensor. A model of the grasp force as a linear function the output of the two strain gages accounted for greater than 90% of the variance of the data when the gage was well mounted and greater than 80% of the variance of the data when the gage was poorly mounted. Including higher-order terms resulted in only a small increase in the variance accounted for by the model. Continued work on optimization of filter order, cut-off frequency, and amplitude thresholds indicated that the gages could be used to detect contact, without detection of false positives, but that the optimal parameters varied across trials, objects, and subjects.

Purpose

The purpose of this project is to improve the function of the upper extremity hand grasp neuroprosthesis by improving user command control. We are specifically interested in designing algorithms that can take advantage of promising developments in (and forthcoming availability of) alternative command signal sources such as EMG, and afferent and cortical recordings. The specific objectives are to identify and evaluate alternative sources of logical command control signals, to develop new hand grasp command control algorithms, to evaluate the performance of new command control sources and algorithms with a computer-based video simulator, and to evaluate neuroprosthesis user performance with the most promising hand grasp controllers and command control sources.

Report of Progress

During this quarter we continued analysis of thumbnail-mounted strain gages as contact and grasp force detectors. As described previously (QPR#4), the output of a metal foil strain gage rosette glued to the thumbnail using cyanoacrylate cement was recorded during grasp, transport and release of a variety of standardized objects. In addition to the standard cylinders and blocks (see QPR#2), trials were also conducted with an instrumented "book" [Memberg and Crago, 1997] which provided a voltage output proportional to the grasp force. Each trial consisted of the subject reaching out, grasping, lifting the object, transporting it to another location 30 cm above the first, and releasing the object. The object was then re-grasped, lifted, and returned to the starting point. Each of 4 subjects completed 4-6 trials with each object and used both lateral and palmar grasp.

USE OF STRAIN GAGE SIGNALS TO MEASURE OBJECT FORCE

As described in our last report (see QPR #5) we are determining the ability of thumbnail-mounted strain gages to measure grasp force. The force was predicted using the output of transversely (T) and longitudinally (L) mounted strain gages as inputs to models fit to the actual grasp force as measured by the instrumented "book". We compared the variance accounted for by different models across two subjects. In the first subject (MMA) the gage was poorly mounted on the thumbnail, while in the second subject (CJP) the gage was well mounted on the thumbnail. The data in Table C.2.b.ii.1 show that the performance of the gage was dependent on mounting, and that higher order terms improved the fit only marginally. Thus, as concluded from our previous analysis (QPR #5), a model of grasp force including linear functions of the transverse and longitudinal strain signals predicts greater than 80% of the variance in the actual grasp force.

communis (EDC), FDS, and flexor digitorum profundus (FDP). The subject had both voluntary and stimulated wrist extension (via residual control and stimulated tendon transfer of the ECU to ECRB respectfully).

Training of Interaction Networks

Interaction networks were designed for grasp force modulation during lateral grasp only. Grasp opening modulation was not tested since EPL stimulation excited the FDS, which resulted in little grasp opening. Lateral grasp was controlled by stimulation of the FDS, FPL/AdP, and ECU. Since only grasp force was modulated, the finger flexor was stimulated at a fixed level.

The arm of the subject was placed in an open cast and held to prevent pronation/supination. The wrist angle was set at 0° prior to stimulation for each trial. Two sets of trials were conducted. In each trial, the pulse width of the ECU was stepped through five values at approximately 5 second intervals, while the FPL/AdP pulse width was fixed at a constant value. In each set of five trials, the FPL/AdP was stimulated at pulse widths of [50, 10, 40, 20, 30 μs] in successive trials. In the first set, ECU was stimulated at [0, 13, 26, 39, 50 μs] and in the second set at [60, 70, 80, 90, 100μs] (data recorded from these trials are displayed in Figure 2.b.iv.1). Note that at pulse widths greater than 50μs, the ECU electrode reached threshold for the supinator. However, pulse widths greater than 50μs were required to achieve adequate wrist extension strength. The stimulation of the FPL/AdP was selected to prevent excitation of the FDS (starting at 60μs). The training data consisted of the wrist angle and grasp force averaged over the last 2 seconds of stimulation at each combination of stimulus parameters.

A 3-layer ANN was constructed both the thumb and wrist modules of the feedforward controller using the MATLAB© Neural Network Toolbox. The input to each neuron is the sum of the weighted outputs of the neurons in the previous layer plus a bias term representing the threshold activation of the neuron. The weights of the ANN were defined as the synaptic strength of the neurons from the input to hidden to output layers respectfully [Rumelhart et al. 1986]. The neuron activation function was a nonlinear sigmoidal function defined as:

$$\text{output} = \frac{1}{1 + e^{-(\text{net input to neuron})}} \qquad (1)$$

The weights and biases were calculated with the back propagation of error algorithm [Rumelhart et al. 1986]. In contrast to the radial basis function network used for the simulation study, this network design allows multiple valued data as part of the training data. To select the number of hidden neurons and the SSE for the back propagation learning algorithm, the ANNs were evaluated on their ability to interpolate between data points. As with the simulations, training data were normalized from -1 to 1.

Evaluation of Feedforward Control Scheme

Once the ANNs were successfully trained, the feedforward controller was assessed in a separate session on its ability to control lateral grasp force and wrist angle. Three separate coordination networks were defined with the following templates: (1) constant wrist angle during changes in grasp force, (2) constant grasp force during wrist extension, and (3) tenodesis grasp. The interaction ANNs of the thumb and wrist module were used to calculate the stimulus pulse widths based on the output of coordination network. Three separate pulse width maps were then pre-programmed with these stimulation values; one for each coordination network. In the actual test session, grasp force and wrist angle were recorded as the muscles were controlled by input commands stepped from 0% to 100% in five increments. Grasp force and wrist angle were calculated by averaging over the last two seconds of stimulation at each level of command. The arm was either held to prevent pronation/supination, or allowed to move freely; the wrist angle was set at 0° at the start of each trial. The controllers were re-tested during the experiment to determine the repeatability of the results.

Measurement of Grasp and Wrist Angle

In both the training and test sessions, grasp force was measured with an instrumented grasp sensor [Memberg and Crago 1995]. The sensor was held between the lateral aspect of the index finger and the thumb with velcro straps and double sided tape. Wrist flexion/extension angle was recorded with a Penny and Giles twin axis goniometer, one end attached to the dorsal side of the hand, and the other end attached

to the forearm. The grasp and wrist data were recorded with a LABVIEW© data collection program at a sampling frequency of 20Hz.

Results

Training Data

Wrist Module In these trials, training data for the wrist and thumb modules were recorded with pronation/supination restricted. At low ECU stimulation levels, the relationship between wrist angle and FPL stimulation was non-monotonic, with FPL stimulation having little effect on wrist angle (Figure 2.b.iv.1). As the ECU stimulation increased, greater wrist extension was possible at lower FPL stimulation levels.

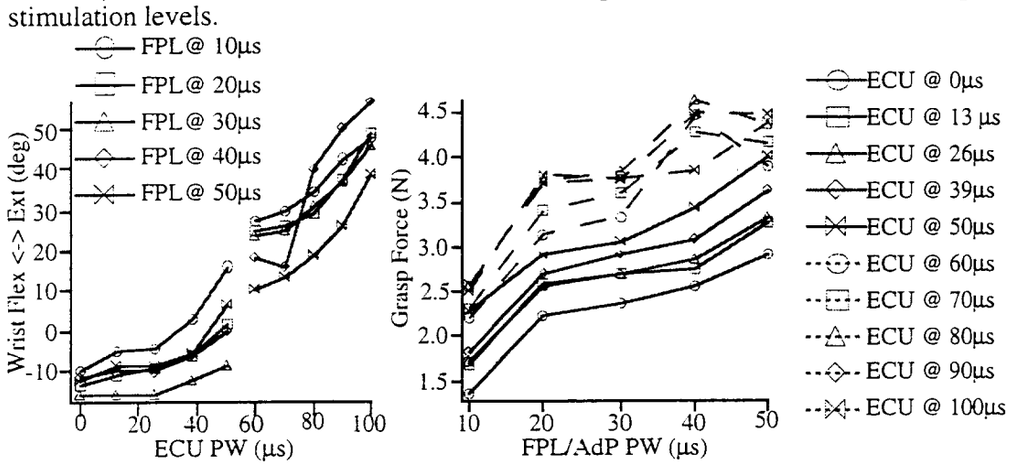

Figure 2.b.iv.1 Training data for wrist module (left) and thumb module (right).

Thumb Module Grasp force was measured as a function of both FPL/AdP and ECU stimulation (i.e. wrist angle). As expected, grasp force increased with FPL/AdP stimulation (Figure 2.b.iv.1). Due to a strong tenodesis pattern, ECU stimulation also increased grasp force. This strong tenodesis pattern (increase grasp force with wrist extension), however, was not seen in the simulations.

Training of Interaction Networks

Some of the data were not included in the training set. For the wrist module, the arm supinated during the trial where the FPL stimulation was at 40µs and the ECU stimulation was increased from 60µs to 100µs. Those data points were not used in the training, due to the strong effects of gravity. Since an unusual amount of wrist flexion was seen during constant FPL stimulation at 30µs as the ECU stimulation increased from 0µs to 50µs, those data points were also not included as part of the training set. All of the other points (total = 65) were used in the training.

The number of hidden neurons and the SSE of the learning algorithm was selected based on the ANN's ability to interpolate between the training points. The stimulation levels from the ANNs were compared to stimulation levels found by interpolating between training points. The best results for both modules were seen when 20 hidden neurons were selected, and the SSE was set to 0.2. The SSE represents the error in normalized stimulation pulse width (0 to 1).

Evaluation of Feedforward Controller

Pulse width maps created by the feedforward controller were used to coordinate the stimulation of the hand and wrist muscles to reproduce a desired lateral grasp and wrist template. Trials were performed with the arm both restricted and free to pronate/supinate. Trials were also repeated to sample the effects of day-to-day variability and time dependent muscle properties.

Constant grasp force during continuous wrist extension. In these trials, a constant grasp force was desired (4N) during wrist extension from -10° flexion (at 0% command) to 30° extension (at 100% command) (Figure 2.b.iv.2). Although grasp force did increase and decrease slightly based on the pattern of FPL/AdP stimulation, force remained relatively constant as the wrist extended (standard deviation of the forces at each command level ranged from 0.2 N to 0.5 N for all trials). Continuous wrist extension was

achieved, although there were small errors between the desired and actual wrist angle. In the repeated trials, the grasp force decreased while wrist extension increased.

The feedforward controller increased ECU stimulation as grasp command increased to produce continuous wrist extension (Figure 2.b.iv.2). FPL/AdP stimulation, on the other hand, decreased as grasp command increased to maintain a constant grasp force as the wrist angle extended.

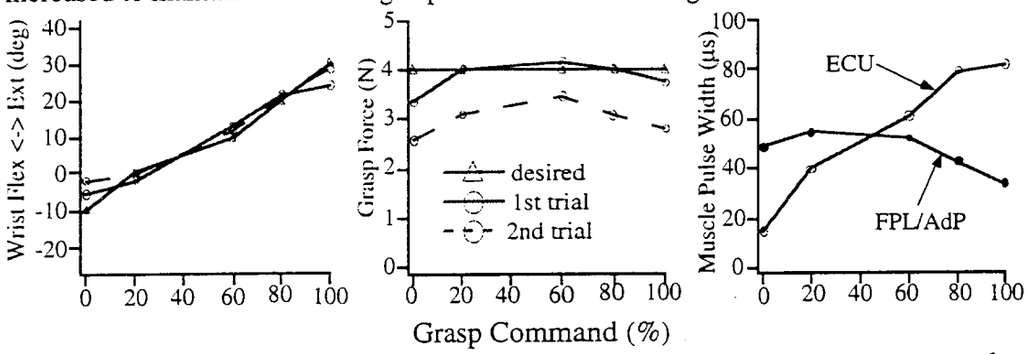

Figure 2.b.iv.2 Clinical evaluation of feedforward controller where a constant grasp force of 4N is desired during continuous wrist extension. Arm held to prevent pronation/supination

Constant wrist angle during changes in grasp force In these trials, a constant wrist angle was desired (-10° flexion, 0°, or 30° extension) during a continuous increase in grasp force (2N to 4N) (Figures 2.b.iv.3). As when a constant grasp force was desired, wrist angle remained relatively constant as the grasp force varied (standard deviation ranged from 0.8° to 5.9° for all trials). Errors between the desired and actual wrist angle were small when constant wrist flexion was desired (Figure 2.b.iv.2), but increased when the desired wrist angle was 0° (Figure 2.b.iv.2). Small wrist angle errors were seen when the desired wrist angle was set at 30° extension (Figure 2.b.iv.2). A continuous increase in grasp force with grasp command was possible for most of the trials. Unlike the constant grasp force templates, both grasp force and wrist extension decreased in the repeated trials (Figure 2.b.iv.3).

To increase grasp force with command, the feedforward controller increased the FPL/AdP stimulation. When wrist flexion, the ECU stimulation remained relatively constant as FPL/AdP stimulation increased (Figure 2.b.iv.2). However, for a desired wrist angle of 0° and 30° extension, ECU was modulated as a function of both wrist angle and FPL stimulation (Figures 2.b.iv.3).

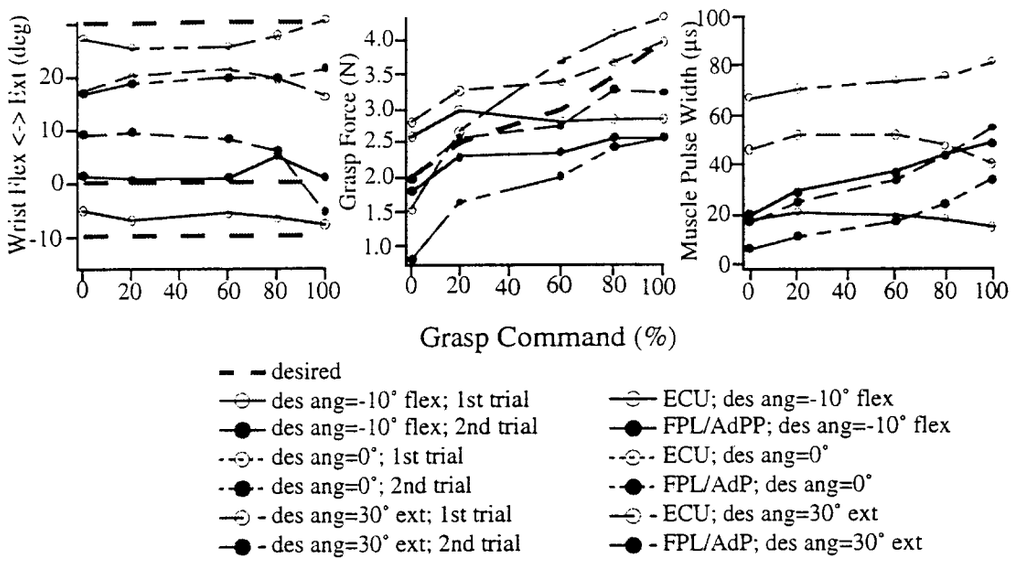

Figure 2.b.iv.3 Clinical evaluation of feedforward controller where a constant wrist angle was desired as grasp force increased with command. Arm held to prevent pronation/supination

Gravitational Effects Most of the trials were performed with both the arm held, and free to pronate/supinate. In all of these trials, ECU stimulation past 50µs excited the supinator, causing unwanted wrist extension when the arm was free to supinate (e.g. Figure 2.b.iv.4). The trial displayed in Figure 2.b.iv.4 was also repeated with the arm pronated. In this instance, gravity was acting in the wrist flexion direction, resulting in unwanted wrist flexion and a decrease in grasp force.

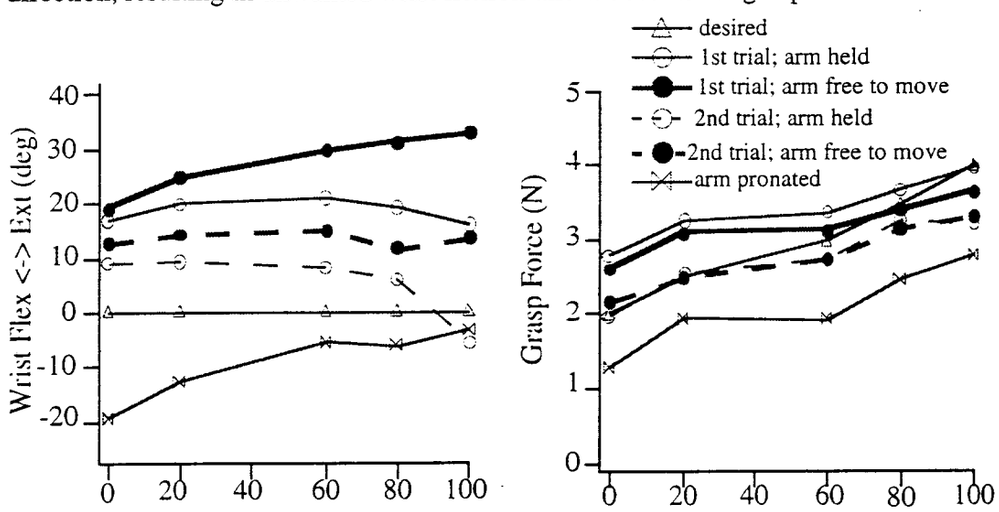

Figure 2.b.iv.4 Effects of gravity on wrist angle and grasp force. Desired wrist angle = 0° as grasp force increased with grasp command.

Tenodesis Grasp A tenodesis pattern of proportionality between wrist extension and grasp force was evaluated (Figure 2.b.iv.5). Wrist extension increased continuously with command; however, wrist flexion at 0% command was not achieved. Grasp force also increased with command, but the majority of the changes occurred at the lower command levels. Both the FPL/AdP and ECU stimulation increased with grasp command to generate changes in both grasp force and wrist angle as a function of command.